Title
Characterizing fibrosis in UUO mice model using multiparametric analysis of phasor distribution from FLIM images.

Journal
Biomedical Optics Express, 7(9)

ISSN
2156-7085

Authors
Ranjit, Suman
Dvornikov, Alexander
Levi, Moshe
et al.

Publication Date
2016-09-01

DOI
10.1364/boe.7.003519

Research Article | Vol. 7, No. 9 | 1 Sep 2016 | BIOMEDICAL OPTICS EXPRESS 3519

Biomedical Optics EXPRESS

Characterizing fibrosis in UUO mice model using multiparametric analysis of phasor distribution from FLIM images

SUMAN RANJIT,[1] ALEXANDER DVORNIKOV,[1] MOSHE LEVI,[2] SETH FURGESON,[2] AND ENRICO GRATTON[1,*]

[1]*Laboratory Fluorescence Dynamics, Department of Biomedical Engineering, University of California, Irvine, CA, USA*
[2]*Departments of Medicine, University of Colorado-Anschutz Medical Campus, Aurora, Colorado, USA*
[*]*egratton22@gmail.com*

Abstract: Phasor approach to fluorescence lifetime microscopy is used to study development of fibrosis in the unilateral ureteral obstruction model (UUO) of kidney in mice. Traditional phasor analysis has been modified to create a multiparametric analysis scheme that splits the phasor points in four equidistance segments based on the height of peak of the phasor distribution and calculates six parameters including average phasor positions, the shape of each segment, the angle of the distribution and the number of points in each segment. These parameters are used to create a spectrum of twenty four points specific to the phasor distribution of each sample. Comparisons of spectra from diseased and healthy tissues result in quantitative separation and calculation of statistical parameters including AUC values, positive prediction values and sensitivity. This is a new method in the evolving field of analyzing phasor distribution of FLIM data and provides further insights. Additionally, the progression of fibrosis with time is detected using this multiparametric approach to phasor analysis.

OCIS codes: (170.2520) Fluorescence microscopy; (100.0100) Image processing; (170.3650) Lifetime-based sensing.

References and links

1. R. Datta, A. Alfonso-García, R. Cinco, and E. Gratton, "Fluorescence lifetime imaging of endogenous biomarker of oxidative stress," Sci. Rep. **5**, 9848 (2015).
2. N. Plotegher, C. Stringari, S. Jahid, M. Veronesi, S. Girotto, E. Gratton, and L. Bubacco, "NADH fluorescence lifetime is an endogenous reporter of α-synuclein aggregation in live cells," FASEB J. **29**(6), 2484–2494 (2015).
3. C. Stringari, R. A. Edwards, K. T. Pate, M. L. Waterman, P. J. Donovan, and E. Gratton, "Metabolic trajectory of cellular differentiation in small intestine by Phasor Fluorescence Lifetime Microscopy of NADH," Sci. Rep. **2**, 568 (2012).
4. C. Stringari, J. L. Nourse, L. A. Flanagan, and E. Gratton, "Phasor Fluorescence Lifetime Microscopy of Free and Protein-Bound NADH Reveals Neural Stem Cell Differentiation Potential," PLoS One **7**(11), e48014 (2012).
5. C. Stringari, H. Wang, M. Geyfman, V. Crosignani, V. Kumar, J. S. Takahashi, B. Andersen, and E. Gratton, "In vivo single-cell detection of metabolic oscillations in stem cells," Cell Reports **10**(1), 1–7 (2015).
6. B. K. Wright, L. M. Andrews, M. R. Jones, C. Stringari, M. A. Digman, and E. Gratton, "Phasor-FLIM analysis of NADH distribution and localization in the nucleus of live progenitor myoblast cells," Microsc. Res. Tech. **75**(12), 1717–1722 (2012).
7. H.-C. Yang, Y. Zuo, and A. B. Fogo, "Models of chronic kidney disease," Drug Discov. Today Dis. Models **7**(1-2), 13–19 (2010).
8. A. Birbrair, T. Zhang, D. C. Files, S. Mannava, T. Smith, Z.-M. Wang, M. L. Messi, A. Mintz, and O. Delbono, "Type-1 pericytes accumulate after tissue injury and produce collagen in an organ-dependent manner," Stem Cell Res. Ther. **5**(6), 122 (2014).
9. R. L. Chevalier, M. S. Forbes, and B. A. Thornhill, "Ureteral obstruction as a model of renal interstitial fibrosis and obstructive nephropathy," Kidney Int. **75**(11), 1145–1152 (2009).
10. A. L. Cochrane, M. M. Kett, C. S. Samuel, N. V. Campanale, W. P. Anderson, D. A. Hume, M. H. Little, J. F. Bertram, and S. D. Ricardo, "Renal structural and functional repair in a mouse model of reversal of ureteral obstruction," J. Am. Soc. Nephrol. **16**(12), 3623–3630 (2005).
11. T. P. Martin, G. Norris, G. McConnell, and S. Currie, "A novel approach for assessing cardiac fibrosis using label-free second harmonic generation," Int. J. Cardiovasc. Imaging **29**(8), 1733–1740 (2013).

Biomedical Optics EXPRESS

12. M. Strupler, M. Hernest, C. c. Fligny, J.-L. Martin, P.-L. Tharaux, and M.-C. Schanne-Klein, "Second harmonic microscopy to quantify renal interstitial fibrosis and arterial remodeling," J. Biomed. Opt. **13**, 054041 (2008).
13. M. Strupler, A. M. Pena, M. Hernest, P. L. Tharaux, J. L. Martin, E. Beaurepaire, and M. C. Schanne-Klein, "Second harmonic imaging and scoring of collagen in fibrotic tissues," Opt. Express **15**(7), 4054–4065 (2007).
14. A. A. Eddy, J. M. López-Guisa, D. M. Okamura, and I. Yamaguchi, "Investigating mechanisms of chronic kidney disease in mouse models," Pediatr. Nephrol. **27**(8), 1233–1247 (2012).
15. C. Arnesano, Y. Santoro, and E. Gratton, "Digital parallel frequency-domain spectroscopy for tissue imaging," J. Biomed. Opt. **17**(9), 096014 (2012).
16. M. A. Digman, V. R. Caiolfa, M. Zamai, and E. Gratton, "The Phasor Approach to Fluorescence Lifetime Imaging Analysis," Biophys. J. **94**(2), L14–L16 (2008).
17. G. I. Redford and R. M. Clegg, "Polar Plot Representation for Frequency-Domain Analysis of Fluorescence Lifetimes," J. Fluoresc. **15**(5), 805–815 (2005).
18. M. Štefl, N. G. James, J. A. Ross, and D. M. Jameson, "Applications of phasors to in vitro time-resolved fluorescence measurements," Anal. Biochem. **410**(1), 62–69 (2011).
19. R. A. Colyer, C. Lee, and E. Gratton, "A novel fluorescence lifetime imaging system that optimizes photon efficiency," Microsc. Res. Tech. **71**(3), 201–213 (2008).
20. F. Fereidouni, A. N. Bader, and H. C. Gerritsen, "Spectral phasor analysis allows rapid and reliable unmixing of fluorescence microscopy spectral images," Opt. Express **20**(12), 12729–12741 (2012).
21. F. Fereidouni, A. Esposito, G. A. Blab, and H. C. Gerritsen, "A modified phasor approach for analyzing time-gated fluorescence lifetime images," J. Microsc. **244**(3), 248–258 (2011).
22. V. Crosignani, A. Dvornikov, J. S. Aguilar, C. Stringari, R. Edwards, W. W. Mantulin, and E. Gratton, "Deep tissue fluorescence imaging and in vivo biological applications," J. Biomed. Opt. **17**(11), 116023 (2012).
23. V. Crosignani, A. S. Dvornikov, and E. Gratton, "Enhancement of imaging depth in turbid media using a wide area detector," J. Biophotonics **4**(9), 592–599 (2011).
24. V. Crosignani, S. Jahid, A. S. Dvornikov, and E. Gratton, "A deep tissue fluorescence imaging system with enhanced SHG detection capabilities," Microsc. Res. Tech. **77**(5), 368–373 (2014).
25. A. G. Lalkhen and A. McCluskey, "Clinical tests: sensitivity and specificity," Continuing Education in Anaesthesia, Critical Care Pain **8**(6), 221–223 (2008).
26. S. Kukreti, A. Cerussi, B. Tromberg, and E. Gratton, "Intrinsic tumor biomarkers revealed by novel double-differential spectroscopic analysis of near-infrared spectra," J. Biomed. Opt. **12**, 020509 (2007).
27. M. Digman, and E. Gratton, "The phasor approach to fluorescence lifetime imaging: Exploiting phasor linear properties," in *Fluorescence Lifetime Spectroscopy and Imaging* (CRC Press), pp. 235–248.
28. P. N. Furness, N. Taub; Convergence of European Renal Transplant Pathology Assessment Procedures (CERTPAP) Project, "International variation in the interpretation of renal transplant biopsies: report of the CERTPAP Project," Kidney Int. **60**(5), 1998–2012 (2001).
29. N. Marcussen, T. S. Olsen, H. Benediktsson, L. Racusen, and K. Solez, "Reproducibility of the Banff classification of renal allograft pathology: Inter- and intraobserver variation," Transplantation **60**(10), 1083–1089 (1995).
30. J. M. Street, A. C. P. Souza, A. Alvarez-Prats, T. Horino, X. Hu, P. S. T. Yuen, and R. A. Star, "Automated quantification of renal fibrosis with Sirius Red and polarization contrast microscopy," Physiol. Rep. **2**(7), e12088 (2014).

1. Introduction

Phasor approach to fluorescence lifetime imaging has been applied to study cellular metabolism and to evaluate presence of reactive oxygen species in living cell and tissue samples [1–6]. This approach is well established for mapping lifetime to a fluorescence image and separating areas of image having distinctively different lifetimes. Recently we have applied this phasor approach to study a combination of lifetime imaging and second harmonic imaging to decipher the extent of fibrosis of the kidney in an unilateral ureter obstruction (UUO) model (manuscript under review) [7–10]. The acquisition of the second harmonic generation originating from the non-centrosymmetric collagen fibers in the tissue is dependent on the direction of the observation. The forward direction acquisition has been shown to be much more sensitive than the backward acquisition of the conventional epifluorescence microscope [11–13]. Thus the forward detection of the harmonic signals is usually done with a modified acquisition scheme in which the detection is performed in the forward direction. The evolution of collagen fibers together with the modification of the tissue architecture due to fibrosis can change the fluorescence lifetime signature of the diseased and normal tissue [8, 10]. These changes in the fluorescence lifetime modify the phasor distribution obtained from the FLIM images and these changes in the phasor distribution can be analyzed and used to separate the diseased from the normal tissue. Furthermore the FLIM data acquisition is independent of the direction of the acquisition (contrary to the detection of harmonics) and thus can be obtained from any laser scanning

Biomedical Optics EXPRESS

microscope equipped with FLIMBOX [14] or other fluorescence lifetime measuring cards and thus this method is applicable in more commonly available instruments. Thus this technique offers a new method where diseased and control tissues are easily separated and the effect of therapeutic interventions can be measured. The main difference of this approach compared to the SHG generation or immunohistochemistry is that this technique does not involve either tissue modification or a specialized instrument. This is a new analysis method which uses FLIM images from any laser scanning microscope capable of fluorescence lifetime imaging and analyzes the phasor distribution originated from the FLIM image to distinguish control and diseased tissues. This paper is focused on the methodology and ideology of this separation and the UUO model of kidney fibrosis was used as a well-studied model of disease progression. This model has been studied in much detail and is known to develop fibrosis over time. Thus we used this method of phasor analysis to separate fibrotic and non-fibrotic samples and show the power and applicability of the technique [14]. The paper uses UUO model as a proven model of fibrosis [14] and thus as a system to show the methodology of this multiparametric analysis when control and diseased sets are known.

In the phasor approach, fluorescence obtained from the tissue following a two photon excitation scheme is transformed to the phasor plot, where each point of an image results in a different phasor point [15–18]. Depending on the tissue architecture and the origin of fluorescence in that particular pixel, different tissues can have differential distribution of the phasor points and the idea in this paper is to use these divergent distributions of phasor points which can be exploited to distinguish diseased from normal tissue and follow the extent of disease progression with time. The phasor histogram and the FLIM images have been analyzed in different ways [16, 19–21]. In the method described in this paper, this distribution of phasor points is split into multiple levels based on the height of peak of the phasor distribution. In each level a number of characteristic parameters of the distribution, including average position, shape, angle and number of molecules in each level are calculated. Finally a spectrum can be constructed from the values of these parameters obtained at the different levels of the phasor distribution. Thus the phasor distribution from FLIM images of each animal contributes to multiple statistical parameters towards the creation of spectrum and creates a specific signature associated with that sample. A comparison between the two spectra comprised of the phasor elements calculated from the diseased and normal tissue samples can thus resolve and distinguish normal and diseased tissue. These comparisons were optimized by using weights whose values can change from 0 to 1. These weights are calculated by maximizing the separation between the control (normal) set of phasor plots and the sample (diseased) set of phasor plots. The weight values are calculated for each of the parameters (e.g. position, shape of distribution, etc.) in a training set and then those values could be used to distinguish the disease progression in unknown samples.

2. Methods

2.1 Unilateral ureteral obstruction model of fibrosis and tissue collection

The animal studies were approved by University of Colorado Institutional Animal Care and Use Committee (IACUC). The University of Colorado animal facility is fully accredited and we followed the National Institutes of Health guidelines for the use of laboratory animals. The experiments use C57/Bl6 6J male mice between 14 and 20 weeks of age. Isoflurane was used as anesthetic, mice were placed prone and chlorhexidine was used to sterilely prep a surgical area. The retroperitoneal area was accessed after a skin incision and after right kidney was exteriorized, the proximal ureter was ligated with a 4-0 silk suture. The wound closed in two layers after the surgical area was cleansed. Kidneys were collected at seven, fourteen, and twenty-one days after the surgery. The left, comparatively uninjured kidneys were used as controls and the right kidneys were used as diseased for each of the time points. The right atrium was cut and mice were perfused with 20 mL phosphate-buffered saline. Kidneys were removed and immersion fixed in 10% formalin for 24 hours. Then kidneys

Biomedical Optics EXPRESS

were processed and embedded in paraffin. 5 μm thick sections were cut onto glass slides. For FLIM imaging, slides were imaged by optical sectioning while embedded in paraffin.

2.2 Data acquisition: description of the DIVER setup used for FLIM

The autofluorescence lifetime of different tissue samples (5 μm thick and embedded in paraffin) were measured using the homebuilt DIVER (Deep Imaging via Enhanced photon Recovery). DIVER is a special modified microscope designed for deep tissue imaging and harmonic imaging [22–24]. The microscope utilizes a forward detection scheme which is very well suited for the harmonic imaging. However, this microscope is also equipped with a FLIMBOX [14] that can acquire fluorescence lifetime data and these FLIM images have been analyzed using the phasor approach to fluorescence lifetime imaging to decipher the extent of fibrosis in the UUO mice model. The construction of this microscope has been explained elsewhere [22–24]. Briefly the samples were excited with 710 nm laser line of a Spectra Physics MaiTai laser using a 20X air objective, and the fluorescence was collected by the large area PMT in the forward direction after passing through an optical filter (410 nm-510 nm) using FLIMBOX which calculates the lifetime from each pixels of the image and transfers the information to the phasor plot directly. The pixel dwell time was 32 μs and the image size was 256x256 pixels with an image size of 360 μm.

2.3 Data analysis

The fluorescence collected from each pixel of the image was transformed to the Fourier space using the following relations:

$$s_i(\omega) = \frac{\int_0^\infty I(t)\sin(n\omega t)dt}{\int_0^\infty I(t)dt}, g_i(\omega) = \frac{\int_0^\infty I(t)\cos(n\omega t)dt}{\int_0^\infty I(t)dt} \quad (1)$$

where, $s_i(\omega)$ and $g_i(\omega)$ are the Y and X coordinates of the phasor plot, respectively; $\omega = 2\pi f$ where f is the repetition frequency of the laser source and n is the harmonic frequency. Thus the fluorescence collected from each pixel of an image is transformed to a point in the phasor plot. Changes in the tissue optical properties due to fibrosis can change the fluorescence lifetime signature of the tissue. The accumulation of collagen and changes in the kidney architecture due to UUO changes the content in the kidney and these changes are reflected in the distribution of the phasor point. In this paper, the primary goal is to use the information about the distribution of the phasor points and predict the behavior of unknown sample.

So far only the average phasor position of a distribution has been used to separate differential behavior of cells undergoing different metabolism or for stem cells undergoing different stages of differentiation [4–6]. However, tissue samples are usually more heterogeneous, have a larger phasor distribution, and thus just the calculation of average phasor positions of the distribution is not enough to distinguish the difference between the samples. Furthermore, often some bright points in the image can dominate the distribution and thus the average g and s coordinates do not have enough sensitivity to distinguish the separation of the normal and the diseased tissue.

To obtain better separation the analysis of the phasor distribution is modified the following way. First, the histogram of phasor points was split in four equidistance segments based on the height of peak of the phasor distribution [Figs. 1(a) and 1(b)]. Then six parameters are calculated for each level. These include the average phasor coordinates g and s, number of points, the shape of the distribution (major axis and minor axis) and the angle of the distribution [θ in Fig. 1(c)]. The shape of the distribution is defined by the length of the long axis of the phasor points (a) and the length of the short axis (b), as shown in Fig. 1(c). The following equations were used for these calculations.

Biomedical Optics EXPRESS

The moment of the distribution was calculated from the position of g and s in the phasor histogram:

$$M_{ij} = \frac{\sum_g \sum_s g^i \cdot s^j \cdot I(g,s)}{\sum_g \sum_s I(g,s)} \tag{2}$$

where, *I(g,s)* is the value of the phasor histogram at position s and g. The phasor histogram has 256x256 bins in the range 0-1 for both the g and s coordinate.

The central moment is calculated from:

$$\mu_{pq} = \sum_g \sum_s \left(g - \bar{g}\right)^p \cdot \left(s - \bar{s}\right)^q f(g,s) \tag{3}$$

where, *p, q*, and *f(g,s)* are the indices indicating the rank of the moment, respectively. We only used moments up to rank 2

The angle is calculated from:

$$\theta = \frac{1}{2} \arctan\left(\frac{2\mu'_{11}}{\mu'_{20} - \mu'_{02}}\right) \tag{4}$$

The shape of the distribution is calculated from value of the major (*a*) and minor axis (*b*):

$$a,b = \frac{\mu'_{20} + \mu'_{02}}{2} \pm \frac{\sqrt{4\mu'^{2}_{11} + (\mu'_{20} - \mu'_{02})}}{2} \tag{5}$$

For the analysis using the Distance program, the measurements are divided in two groups that we call F and C, representing the training sets for two conditions to be separated. For each member of a training set we measure the pixel phasor distribution, i.e., the phasor plot for that member and we use the method of analysis of the phasor distribution defined by [Eqs. (2)-(5)]. This procedure gives for each measurement k a spectrum *f(i,k)* made of 24 points. For the 2 groups F and C we calculate the average spectrum of the group and the deviation of each member from the average as shown in Eq. (6) for the group F

$$DF_F(k) = \frac{\sum_i \left(F_{av}(i) - f(i,k)\right)^2 w(i)}{N} \tag{6}$$

where the sum is over the *N* points of the spectrum and *k* is the index for a given measurement. For the same member we also calculate the distance from the average of the other group C,

$$DF_C(k) = \sum_i \left(C_{av}(i) - f(i,k)\right)^2 w(i) \Big/ N \tag{7}$$

The same calculation is performed for the members of group C so that we will have the distance DC_C and DC_F. The weights *w(i)* are quantities that can vary between 0 and 1 and they are normalized so that the sum of all weights is a constant. These weights are used to emphasize which one of the spectral points is more important to achieve the separation of the two groups since we don't know which of the points in the spectrum is important. For determining the weights *w(i)* we build the following quantity that we call Distance D

$$D = \min\left[\sum_k \left(DF_F(k) + \frac{1}{DF_C(k)} + DC_C(k) + \frac{1}{DC_F(k)}\right)\right] \tag{8}$$

where *w(i)* are weights to be determined by the minimization algorithm. If $w_i = 0$, the corresponding spectral point does not influence the distance D. If *w(i)* = 1 it has a maximum influence. What this algorithm achieves is to find the parameters *w(i)* for the training set than

Biomedical Optics EXPRESS

minimize the distance between the points of a set from the average of the set and maximize the distance from the average of the other set. The operator can set some of the weights to zero effectively removing that spectral point from D. This calculation is done only for the training set. After minimization, we have the values of the weights that best separate the two groups of the training set. By setting some of the weights = 0 we could test if the selected points in the spectra give a significant contribution to the separation of the two sets. The *w(i)* values are stored and associated with a given training set together with the average spectrum of the set F and of the set C. This is all we need to measure the position of an unknown sample with respect to the training set. This position is obtained using the separation index SI defined as

$$SI(k) = 10 \times \frac{\left(DX_C(k) - DX_F(k)\right)}{\left(DX_C(k) + DX_F(k)\right)} \tag{9}$$

where X is a measurement to be indexed. In few words, if the spectrum of X is equal to the average of C then SI = −10 and if it is equal to the average of F then SI = + 10. If the spectrum is at equal distance from C and F then SI = 0.

Using the SI index for the spectra of the training set we can build the SI histogram and determine if a member is a true positive (below 0) or a false positive (above 0). After this maximization algorithm is employed the following parameters are calculated: AUC or area under the curve, False positive rate, True positive rate, Accuracy of the measurements, Precision or positive prediction value, Sensitivity and Specificity [25].Statistical methods such as the area under the curve (AUC) are then used to determine the quality of the training set. The Distance approach has been used previously to determine the separation of spectra in human cancer tissues [26].

This multiparametric FLIM was first used to separate the most diseased 21 day right kidney and the most normal 7 day left kidney samples and calculate the values of the weight parameters for each point of the spectrum. Then the unknown samples, including partially diseased 7 and 14 day right kidneys and comparatively healthier 14 and 21 day left kidney samples were compared with these two sets to calculate the extent of the disease (fibrosis in this case) progression. The histogram separating the normal and disease tissue was plotted in a scale of −10 to + 10. The best separation is obtained when the control set is at −10 and the diseased set is at + 10. These plots show how well the images from one sample can be separated from the images from the other samples in terms of their lifetime distribution in the phasor plot.

Biomedical Optics EXPRESS

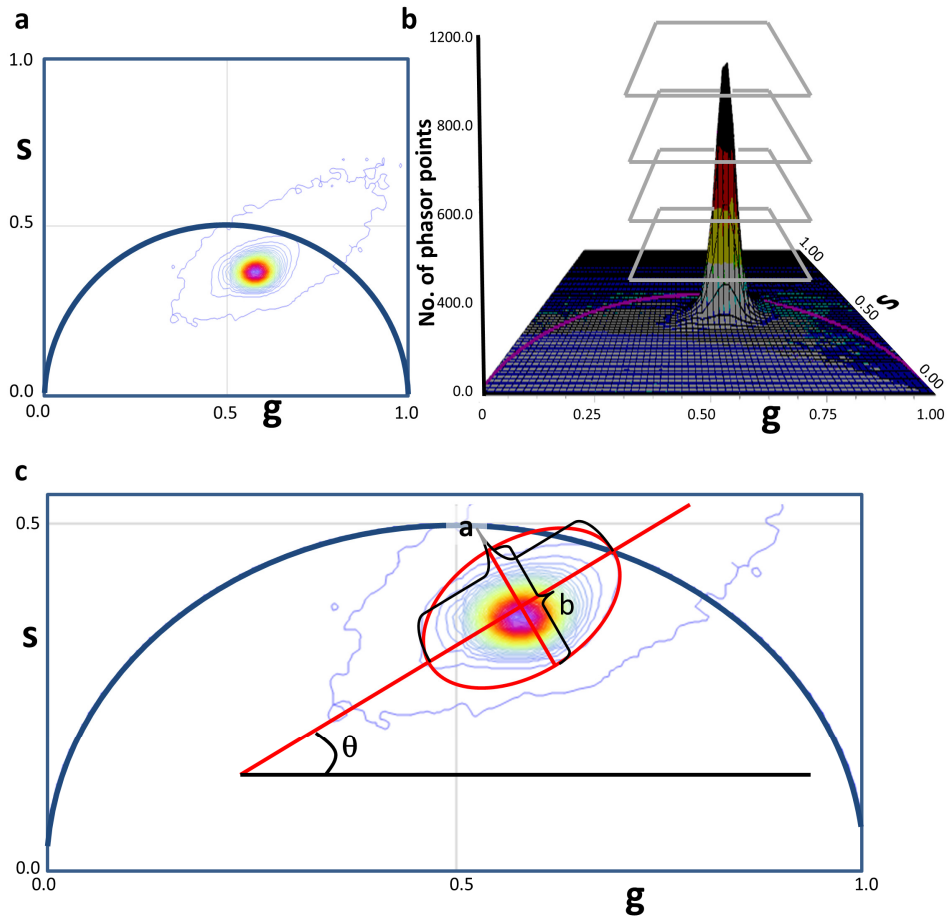

Fig. 1. (a) The distribution of the phasor points in the phasor plot as a heat map. (b) The distribution of phasor point according to number of points and splitting of the points in four equal heights, starting at zero height. (c) The calculation of the shape of phasor distribution (a and b, the long and short axes, respectively) and the angle of the distribution (θ).

3. Results

3.1 FLIM and phasor signature of the UUO samples

Fluorescence lifetime images having an image size of 360 µm were obtained for each animal. Ten images were taken for each kidney. The left kidneys were used for the control and the right kidneys were used for the diseased samples. Images were obtained for eight animals at each time point. Examples of the images from control left kidney (top) and diseased right kidney (bottom) for 7, 14 and 21 days of UUO are shown in Fig. 2(a). The images were color mapped according to the color distribution shown in the phasor distribution of Fig. 2(b). The differences in the images clearly show that the tissue is different for the control and the diseased tissue at each time point. The distribution of phasor points along the line joining cursor 1 (red) and cursor 2 (green) can be converted to the fraction of species at cursor 2 (green) by using the method of phasor addition [27]. The two cursors were arbitrarily chosen to show the continuous color scale. These distributions show that although there are noticeable differences between the images of the control and diseased kidney, the overall distribution of phasor points do not have any systematic difference that can be used to separate diseased from the control tissues [Fig. 2(c)]. Figure 2(d) shows the phasor histograms from Normal (top) and diseased (bottom) kidney of 7, 14 and 21 day (left to

Biomedical Optics EXPRESS

right). It is evident from the histograms, that calculation of average phasor positions are not enough for the separating the normal from diseased tissues. This is the reason the phasor analysis in this paper has been modified to distinguish the two types of tissues.

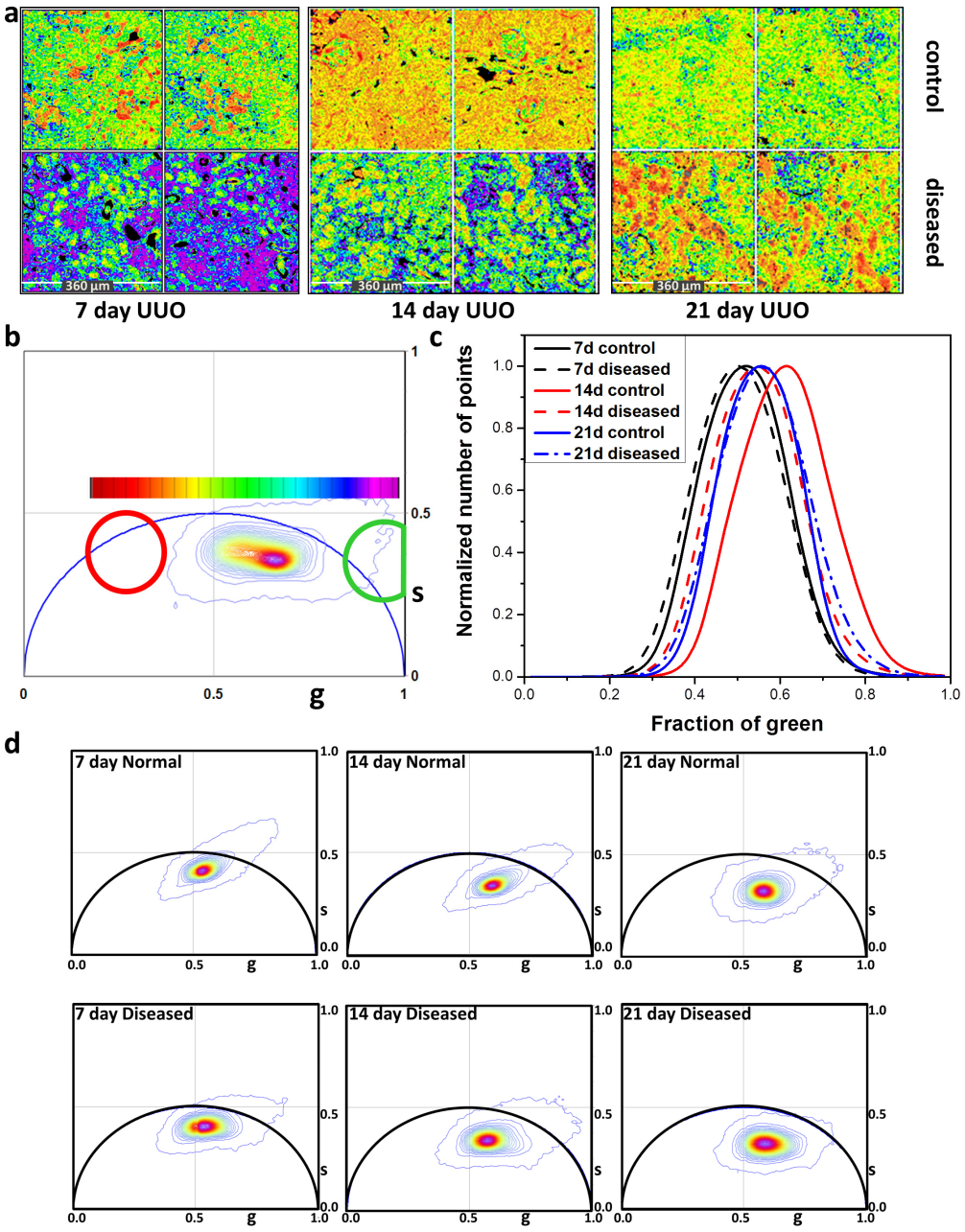

Fig. 2. (a) The color mapped FLIM images of the control (top) and diseased tissue (bottom) at different time points of UUO. (b) The phasor distribution of the FLIM images from the kidney and the color map used for color mapping images in Fig. 2(a). (c) The distribution of phasor points along the line joining the red and green cursor in Fig. 2(b). The distributions for control (solid) and diseased (dashed) tissue samples at 7 day (black), 14 day (red) and 21 day (blue) are shown. (d) The phasor histograms from representative samples of 7 day, 14 day and 21 day (left to right) normal (top) and diseased kidney (bottom) of the same animal.

Biomedical Optics EXPRESS

3.2 Separation of control and diseased samples and calculations of ROC curves

The comparative analysis was done by comparing the most normal 7 day left kidney FLIM images and the most fibrotic 21 day right kidney FLIM images. The 7 day left kidney images were used as the control set and the 21 day right kidney images were used as sample set. Each of these sets included images from 8 different mice kidneys and 10 different FLIM images from each of these mice. We wanted to use the least amount of parameters required to separate the control and the sample set and hence used 5 parameters (*g, s, a, b, θ*) for the separation. The plot of true positive rate against false positive rate for this set [blue in Fig. 3(a)] gives an AUC value of 0.957, determining the very good separation this method can achieve. This separation has a very small false positive rate of 0.079 and a positive prediction value of 0.923. This result shows the sensitivity and specificity that can be obtained by this analysis technique while separating the disease from the control tissue. We also compared how well we can separate the healthy 7 day left kidney samples from comparatively diseased 7 and 14 days of UUO right kidneys. Figure 3(a) shows the ROC curves for comparisons between 7day left and 7 day right (black) and 14 day right (red) kidneys. A comparison of the AUC values show the most fibrotic 21 day right kidney has the best separation (AUC = 0.957) and the separation becomes worse for the 14 day right (AUC = 0.845) and it is the worst for the 7 day right kidney (AUC = 0.646). The corresponding false positive rate and positive prediction values along with specificity and sensitivity are given in the Table 1. The separation obviously becomes better as the time of UUO progresses. The other pairwise comparison we wanted to carry out is to see how the phasor distributions of the comparatively healthy left kidneys differ from the diseased right kidneys at the same time point of UUO. These comparisons are shown in Fig. 3(b) and the ROC curves are best for the 21 day of UUO [blue in Fig. 3(c)] and are worse for the 7 day (black) and 14 days of UUO (red). These show how the obstructed right kidneys are very fibrotic on 21 days of UUO but are much less fibrotic before.

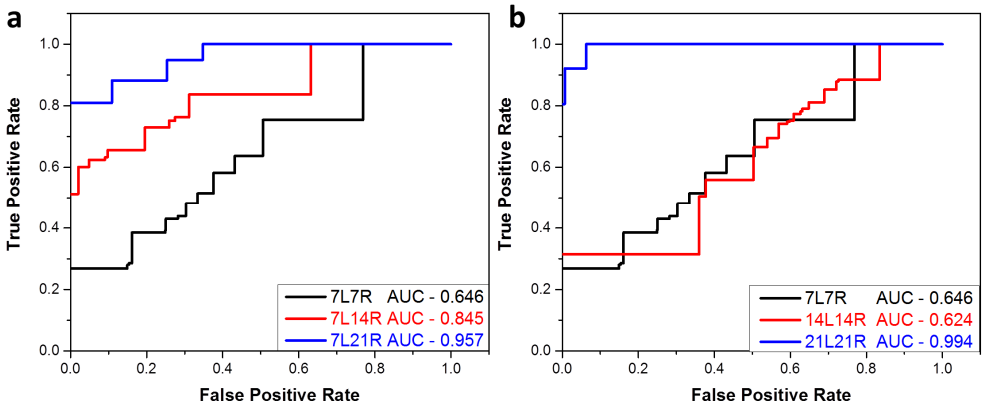

Fig. 3. (a) ROC curves for the separation of the most normal 7 day left kidney and 21 day right kidney (blue), 14 day right kidney (red) and 7 day right kidney (black). (b) ROC curves for the comparison of comparatively healthy left kidney and diseased right kidney at different time points of UUO (7 day – black, 14 day – red and 21 day - blue).

Biomedical Optics EXPRESS

Table 1. Statistical parameters calculated from the ROC curves

Control	Sample	AUC value	False positive rate	True positive rate	Positive prediction value	Sensitivity	Specificity
7L	7R	0.646	0.061	0.813	0.949	0.813	0.939
7L	14R	0.845	0.109	0.878	0.923	0.878	0.891
7L	21R	0.957	0.079	1.000	0.923	1.000	0.921
14L	7R	0.627	0.257	0.619	0.672	0.619	0.743
14L	14R	0.624	0.271	0.724	0.724	0.724	0.729
14L	21R	0.889	0.047	0.859	0.948	0.859	0.953
21L	7R	0.579	0.384	0.553	0.600	0.553	0.616
21L	14R	0.960	0.000	0.543	1.000	0.543	1.000
21L	21R	0.994	0.000	0.500	1.000	0.500	1.000
7L	14L	0.698	0.410	0.696	0.688	0.696	0.590
7L	21L	0.926	0.000	0.533	1.000	0.533	1.000

3.3 Following evolution of fibrosis with time of UUO

In UUO mice model the kidney with the obstruction (right kidney in these experiments) develops extensive fibrosis over time. The increase in fibrosis is dependent on the time of UUO. Amount of collagen fibers increases over time and tissue architecture also undergoes progressively more changes [8, 10]. Thus the lifetime signature and hence phasor distribution changes increasingly as time of UUO continues. A second hypothesis is that over time there are changes in the tissue architecture in comparatively healthy left kidney also. In absence of a fully functional right kidney, left kidney of an UUO animal is used more than the left kidney of a fully healthy mouse (hyperfiltration, etc.). Thus overtime the left kidney can also become diseased. Our goal was to follow the progression of UUO using the phasor distribution and study the evolution of the disease in both kidneys with time of UUO. To achieve this, the healthy 7 day left kidney phasor distributions were used as the control and the phasor distributions of fibrotic 21 day right kidneys were used as the sample. Then five parameters (g, s, a, b, θ) were used for the separation of the spectra obtained from these two sets. The values of the weight were obtained for each point of the spectra, i.e. the twenty points originating from four layers of phasor distribution. Then these values of the weights were used to calculate how the unknowns i.e. the 7 and 14 day right kidney samples and 14 and 21 day left kidney samples separate from the healthy and diseased tissues. The comparison between the 7 day left (black) and 21 day right kidney samples (red) are shown in Fig. 4(a). The complete separation between the samples shows the power of this multiparametric analysis to decipher the extent of fibrosis from the FLIM images. The separation analyzed using the value of the weights obtained for Fig. 4(a) shows that fibrosis increase from 7 day right (magenta) to 14 day right (blue) to 21 day right (red) in Fig. 4(b). Similar trait is observed for the 14 day left (violet) and 21 day left (green) kidney samples [Fig. 4(c)]. However the left kidneys are more similar to 7 day left kidney and the extent of fibrosis in the left kidney tissues are much lower. These results prove the hypothesis that there is a progressive evolution of fibrosis in the obstructed kidney of the mouse with time and the

Biomedical Optics EXPRESS

relatively healthy left kidneys [Fig. 4(c)] also become diseased, albeit to a much less extent [Fig. 4(b)] This shows how this multiparametric phasor analysis can enable us to follow fibrosis in UUO mice model.

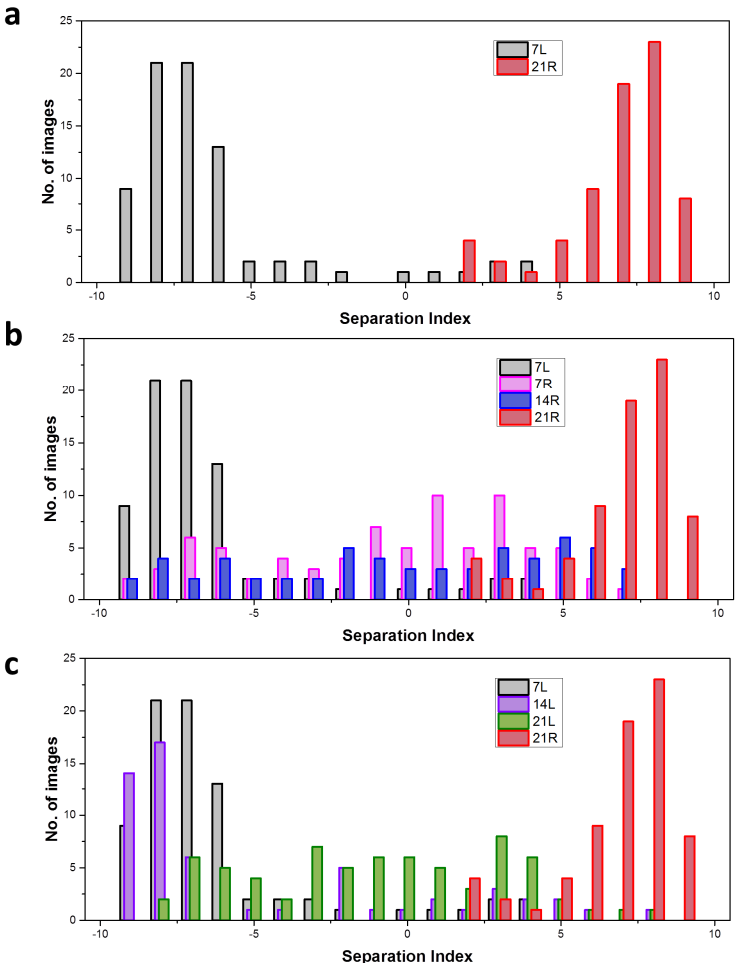

Fig. 4. Plot of number of images against separation index. The separation index has a value of –10 to + 10. (a) The separation between 7 day left (black) and 21 day right (red) shows the efficiency of this analysis to separate the diseased and normal tissue. (b) The evolution of fibrosis in the right kidney with time of UUO (purple-7R, blue – 14 R and red – 21R) compared to the 7 day left (black). (c) Similar plot for the fibrosis in left kidneys (black – 7L, violet – 14L, green – 21L, and red – 21R).

4. Discussion

UUO model of kidney fibrosis is a well-studied model for fibrosis evolution in mice kidneys. The obstruction of the ureter increases tubular pressure, reduces glomerular filtration rate, and activates many vasoactive hormones and cytokines through the kidney leading to fibrosis over time. The increasing amount of collagen as the disease progresses can be quantified by staining, immunohistochemistry or second harmonic generation (SHG) microscopy. Staining by Picrosirius red or Masson Trichrome requires tissue modifications and is dependent on the pathologists [28–30]. Immunohistochemistry depends on development of specific antibodies for each antigen and can produce variable results. SHG imaging, as mentioned earlier, is much better suited for the forward detection and usually requires a modified laser scanning microscope construction. The power of FLIM methodology is in the automated analysis

Biomedical Optics EXPRESS

which does not need an intervention from a pathologist. This can greatly reduce the time and cost of the understanding in fibrosis at the initial stages. These experiments and analysis have been performed on 5 µm slices. However, in an epifluorescence microscope equipped with FLIM capability these measurements can be carried out close to the surface with optical sectioning. SHG generation in forward direction is harder to acquire in thick tissue samples and thus this method have a much higher potential to be used in the thick samples.

A method of studying fibrosis was developed in this work by analyzing the fluorescence lifetime images and the phasor approach to lifetime imaging. This multiparametric analysis of phasor histogram does not require any special laser scanning microscope. Any laser scanning fluorescence microscope equipped with either FLIMBOX or any other fluorescence lifetime measuring card can be used to acquire fluorescence lifetime images and can be converted to a distribution in the phasor plot. The main goal of this paper is to quantitatively distinguish healthy tissue from the diseased fibrotic tissues using the phasor distribution. The calculations of just the average positions of the phasor coordinates were not enough to distinguish the changes in the tissue signature due to fibrosis. The AUC value obtained between the least fibrotic 7 day normal kidney and the most fibrotic 21 day right kidney from the comparison of just the two parameters g and s using the method described in this paper is 0.865. This value improves to 0.957 when five parameters were used, demonstrating the power of this analysis. Thus the analysis of the phasor distribution was enhanced to calculate multiple parameters and create a spectrum involving those parameters. Comparisons between spectra from different samples required use of weights for each parameter and to identify the best separation between the control and diseased samples. Weights for each parameter were calculated using the healthiest 7 day left and the most diseased 21 day right kidney. These same weights are then used to evaluate the separation index for the tissue samples with unknown extent of disease. The results show that the UUO-induced fibrosis progresses with time and the progression is faster for the obstructed right kidney compared to the unobstructed left kidney.

Funding

National Institutes of Health (NIH)-P41 GM103540, NIH-P50 GM076516, NIH K08 HL103774, VAMR 1I01BX001954, NIH 1R01DK098336 to M. L.

Acknowledgment

We thank Milka Stakic for technical assistance.